Chapter 3

Cation Disorder in $MgAl_2O_4$ Spinel

Much of the work presented in this chapter has previously been published in the Journal of Physics: Condensed Matter [97]

3.1 Introduction

Magnesium aluminate ($MgAl_2O_4$) spinel has demonstrated a strong resistance under irradiation to the formation of large defect aggregates such as dislocation loops and voids [39]. Given this resilience, the likelihood of radiation induced swelling and microcrack formation is dramatically supressed. Consequently $MgAl_2O_4$ has the ability to withstand neutron irradiation over a wide temperature range without degradation of its mechanical proper-

ties [98–100], conversely it does amorphize under fission tracks [101]. Spinel is therefore being considered for applications which would exploit its specific radiation tolerance. These include use as an insulating and structural material in fusion reactors [102] and as an inert matrix target material in the nuclear transmutation of radioactive actinides [103, 104].

The ability of spinel to tolerate radiation damage is thought to be a result of two factors. The first is a high interstitial-vacancy (i-v) recombination rate [39]. The second factor is the ability of the lattice to tolerate significant intrinsic antisite disorder on the cation sub-lattice [105–107] as described by equation 3.1.

$$\mathrm{Mg}_{\mathrm{Mg}}^{\times} + \mathrm{Al}_{\mathrm{Al}}^{\times} \rightarrow \mathrm{Mg}_{\mathrm{Al}}^{\prime} + \mathrm{Al}_{\mathrm{Mg}}^{\cdot} \tag{3.1}$$

This is supported by neutron diffraction data from stoichiometric spinel, which demonstrated significant cation disorder in a sample exposed to a high radiation dose (249 dpa at 658 K) [39]. Recent atomistic simulations of displacement cascades in spinel also resulted in high concentrations of cation antisite defects, often grouped as clusters [108]. It is, however, difficult to correlate such simulation results directly with the experimental data. One therefore needs an observable, related to defect formation, that can be calculated in a simulation and used to evaluate the efficacy of the method.

The cation distribution in spinels and in $MgAl_2O_4$ in particular has been the subject of several simulation studies [109–113]. Parker [109] used a Mott-Littleton methodology similar to that described in section 2.7 to predict the preferential structures for 18 spinels including $MgAl_2O_4$. Cormack *et*

al. [110] also predicted the structures of these 18 spinels using a Buckingham potential model. In analysing their results they considered a range of effects to be important, these are: Electrostatic and short-range contributions, ion size, crystal field effects, coordination number and ordering of cations. Grimes *et al.* [111] used a normalised ion energy method to predict cation distributions for 50 spinels again including $MgAl_2O_4$ and showed that it was possible to predict the normal/inverse preference of these materials by considering the anion and cation preference energies. Wei and Zhang [112] studied the cation distribution in a range of spinels using density functional theory (DFT). By calculating the Madelung constant for these spinels they showed that a knowledge of the value of the u parameter alone is not sufficient to predict the normal/inverse preference as had been assumed in some previous work [23]. They also showed that the band gap in these materials can change significantly based on wether they take a normal or inverse structure. A recent publication by Seko *et al.* [113] uses DFT and configurational averaging to study volume change as a function of inversion in several spinel, finding good agreement with calculations discusses later in this chapter.

3.1.1 Crystal Structure

The structure of normal spinel is shown in figure 3.1. If the O^{2-} ions are considered to form a face centred array, within the unit cell, Mg^{2+} ions occupy tetrahedral interstices between O^{2-} ions, the smaller Al^{3+} ions are sited in octahedral interstices. These cation sublattices only partly fill the

available interstices and the remaining positions are generally considered to accommodate interstitial ions [114].

From a formal crystallographic point of view spinel exhibits a face centered cubic Bravais lattice with space group F$\bar{4}$3m [115], though the more simple Fd3m is usually assumed [39], the differences in atomic positions between the two groups being small. In this Mg^{2+} ions occupy perfect tetrahedral 8a symmetry positions and Al^{3+} ions perfect octahedral 16d sites (as in figure 3.1, a list of coordinates is provided in table 3.1).

Table 3.1: Perfect lattice positions in normal $MgAl_2O_4$ assuming space group Fd3m and the origin at $\bar{4}$3m.

Species	Wyckoff position	Fractional coordinates
Mg	8a	0,0,0; $1/4, 1/4, 1/4$; F.C.
Al	16d	$5/8, 5/8, 5/8$; $5/8, 7/8, 7/8$; $7/8, 5/8, 7/8$; $7/8, 7/8, 5/8$; F.C.
O	48f	$u, 0, 0$; $\bar{u}, 1/2, 1/2$; $0, u, 0$; $1/2, \bar{u}, 1/2$; $0, 0, u$; $1/2, 1/2, \bar{u}$; $3/4, u + 1/4, 3/4$; $1/4, \bar{u} + 1/4, 1.4$; $u + 3/4, 3/4, 1/4$; $\bar{u} + 3/4, 3/4, 1/4$; $3/4, 1/4, \bar{u} + 3/4$; $1/4, 3/4, u + 3/4$; F.C.

Within space group Fd3m the O^{2-} anions occupy 48f positions which are characterised by the oxygen positional (u) parameter, which is a measure of how far they are displaced, in $\langle 111 \rangle$ directions, from ideal FCC positions.

Although the observed u parameter is a function of how the spinel was processed, it generally corresponds to a displacement of approximately 0.1Å. This shift is away from the divalent Mg^{2+} ions and thus represents a volume expansion of the tetrahedral sites at the expense of octahedral site volume. The view of spinel as a perfect FCC arrangement of anions (as in figure 3.1) is therefore overly simple.

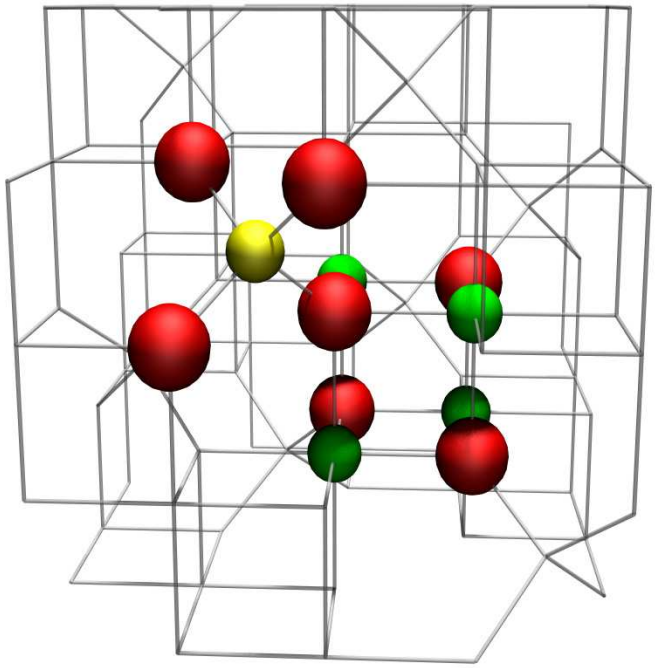

Figure 3.1: A single unit cell of normal $MgAl_2O_4$ spinel showing a tetrahedral Mg^{2+} coordinated by four O^{2-} ions corner linked to a cube composed of four octahedral Al^{3+} and four O^{2-} ions.

3.1.2 Inversion Parameter

The extent to which the cation sub-lattice is disordered (as in equation 3.1) is quantified by the inversion parameter i; the fraction of Al^{3+} cations occupying tetrahedral sites. As such, i can vary from 0, which correlates to a perfect normal spinel with all Mg^{2+} atoms on tetrahedral lattice sites, to 1 which refers to an inverse structure where all tetrahedral lattice sites are occupied by Al^{3+} ions. This is formally expressed as $(Mg_{1-i}Al_i)[Mg_iAl_{2-i}]O_4$ where parentheses refers to the tetrahedral sites and square brackets to the octahedral sites.

It only requires a few minutes of equilibrating synthetic samples at high temperatures followed by quenching to induce sufficient cation exchange to raise the inversion parameter from 0.1 to values between 0.2 and 0.6 [116]. The variation of lattice parameter with respect to disorder has been shown to be small: a change in i of 0.1 modifies the lattice parameter by just 0.0025 Å [117, 118].

Natural spinel, which has been able to equlibriate over geological timescales, might be expected to have a value of i approaching 0. This is somewhat reflected in the literature where experimental inversion parameters vary in the range $0.025 \leq i \leq 0.12$ [26, 33, 34]. Unfortunately none of these studies reported an associated lattice parameter. Conversely the study of Hafner *et al.* [28] reports the lattice parameter of natural spinel to be 8.089 ± 0.0005 Å but gave no indication as to the degree of inversion. When the predictions made here are compared to this lattice parameter an inversion in the range

0.025 - 0.12 is assumed.

Given the discussion of the u parameter in section 3.1.1 it might also be expected that value of this parameter will vary with the degree of inversion. As with the lattice parameter the variation in u parameter with inversion is small, a change in i of 0.1 modifying the u parameter by 0.0015 lattice units. Sickafus *et al.* [38] proposed an empirical model to describe this relationship, this is defined as equation 3.2.

$$u = 0.3876 \left(\frac{\langle r(B) \rangle}{\langle r(A) \rangle} \right)^{-0.07054} \tag{3.2}$$

where $\langle r(A) \rangle$ and $\langle r(B) \rangle$ are the average radii of the ions on the A and B lattice sites (note: a different origin has been used and a translation to $(-\frac{1}{8}, -\frac{1}{8}, -\frac{1}{8})$ must be performed to obtain values consistent with the ones used here).

3.1.3 Order-Disorder in $MgAl_2O_4$

Disorder in $MgAl_2O_4$ has been observed in a number of experimental studies, for example, [24, 117, 119, 120]. Here it is examined using a variety of analyses, including a mean-field approach, the calculation of defect volume and a novel combined energy minimisation - Monte Carlo (CEMMC) technique [12, 69]. In all these cases, the simulations use energy minimisation techniques and effective potentials to describe the forces between ions. The potentials were derived by fitting to room temperature structural data taken

from a number of materials including MgO, Al_2O_3 and perfect $MgAl_2O_4$ (extrapolated from ref [117]). Consequently we compare our results to the quenched room temperature experimental data of Andreozzi *et al.* [117] and Docherty *et al.* [118] on synthetic materials and the derived data described above on natural spinel [28].

3.2 Predicting Structural Parameters as a Function of Disorder Using Pair Potentials

The four methods employed for calculating lattice parameter as a function of defect concentration are now reviewed. Additionally two of these will be used to model the variation in the u parameter as i is increased.

The Buckingham potential parameters used throughout this chapter are listed in table 3.2

Table 3.2: Short-range potential parameters.

Species	A(eV)	ρ(Å)	C(eV.Å^{-6})
$O^{2-}-O^{2-}$	9547.96	0.21916	32.00
$Mg^{2+}-O^{2-}$	1279.69	0.29969	0.00
$Al^{3+}-O^{2-}$	1361.29	0.3013	0.00

A shell model, as described in section 2.5 is used for the O^{2-}-O^{2-} interaction; the relevant parameters are reported in Table 3.3.

Table 3.3: Shell model parameters.

Species	Y(eV)	k(eV.Å^{-2})
O^{2-}	-2.8	54.8

3.2.1 Periodic Pair Potential Calculations

As described in section 1.1.1 a perfect lattice is described by identifying the ion positions within a unit cell and then repeating this through space using periodic conditions. If, in a single unit cell consisting of 56 atoms, all tetrahedral sites are occupied by Mg^{2+} cations this results in a zero inversion (i=0) perfect lattice. If one Mg^{2+} tetrahedral cation is swapped for a near neighbour octahedral Al^{3+} cation, by virtue of the periodic conditions, we have introduced a degree of disorder into the lattice corresponding to the value i=0.125. If two adjacent pairs are swapped i=0.25 and if three adjacent pairs i=0.375. There is only one distinct way of arranging a nearest neighbour antisite cluster. For the larger clusters of two and three nearest neighbour antisite pairs the defects can be placed in multiple distinct arrangements. The defect coordinates used in this study are listed in table 3.4.

Through energy minimisation these calculations therefore provide us with four values of the spinel lattice parameter corresponding to four values of inversion parameter. Inherent in these calculations are intra cluster defect - defect interactions, albeit specific to these cluster configurations. In addition, because of the periodic conditions, there are inter-cluster-cluster interactions.

The periodic pair potential calculations described in this chapter were per-

Table 3.4: Defect coordinates for arrangements of 2 and 3 antisite pairs.

Configuration	Defect species	Wyckoff position	Defect coordinates
$2\{Al^{\cdot}_{Mg}{:}Mg'_{Al}\}$	$Al^{\cdot}_{Mg}$	8a	$1/4, 1/4, 1/4;$
			$3/4, 1/4, 3/4$
	$Mg^{\cdot}_{Al}$	16d	$5/8, 1/8, 1/8;$
			$3/8, 1/8, 7/8$
$3\{Al^{\cdot}_{Mg}{:}Mg'_{Al}\}$	$Al^{\cdot}_{Mg}$	8a	$0, 1/2, 1/2; 1/2, 0, 1/2;$
			$1/2, 1/2, 0$
	$Mg^{\cdot}_{Al}$	16d	$5/8, 1/8, 1/8; 1/8, 5/8,$
			$1/8; 1/8, 1/8, 5/8$

formed with the CASCADE code [121].

3.2.2 Calculation of Defect Volumes

Local relaxations induced by defects can generate a significant expansion or contraction of the unit cell. This change in volume is specific to the type of defect and can be modelled by application of the following formula [122–124]:

$$\nu = -K_T V_c \left(\frac{\partial f_v}{\partial V_c}\right)_T, \tag{3.3}$$

where K_T ($\text{Å}^3\text{eV}^{-1}$) is the isothermal compressibility V_c (Å^3) is the unit cell volume of the perfect lattice and f_v is the internal defect formation energy calculated within the Mott-Littleton approximation.

For a cubic system, the isothermal compressibility is readily obtained from

equation 3.4 [125],

$$K_T = [1/3(c_{11} + 2c_{12})]^{-1} \tag{3.4}$$

where c_{11} and c_{12} are the calculated elastic constant matrix elements (table 3.5). The partial derivative in equation 3.3 is determined numerically by conducting a series of constant volume calculations. (described in section 2.6. The equilibrium lattice parameter for $MgAl_2O_4$ is found to be 8.090 $\mathring{A}$ thus constant volume calculations were performed for the range $8.020 \leq a \leq 8.160\mathring{A}$ The final unit cell volume can be established by adding the defect volumes for a given defect concentration (equivalent number of defects in a unit cell) to the perfect unit cell volume.

$$\text{Defective unit cell vol.} = \Sigma(\nu\times \text{ Number of defects per unit cell}) + V_c \tag{3.5}$$

where the defect volume, ν, is evaluated from equation 3.3. Thus, a prediction of the defect volumes generates a linear change in lattice parameter as a function of defect concentrations (inversion).

Table 3.5: Elastic constants and isothermal compressibility for $MgAl_2O_4$.

	Experiment [126]	Predicted
c_{11}	$\sim$ 299 GPa	367.5 GPa
c_{12}	$\sim$ 153 GPa	234.8 GPa
K_T	$\sim 5.00\text{x}10^{-4}\mathring{A}^3\text{eV}^{-1}$	$\sim 8.60\text{x}10^{-4}\mathring{A}^3\text{eV}^{-1}$

Since defect energies are calculated at the (Mott-Littleton) dilute limit a potential problem with this technique is that we completely neglect the effect of defect-defect interactions, which are likely to become increasingly

important at elevated degrees of disorder. Therefore, we use the same technique, but consider the defect volume created by an adjacent pair of defects $\{Mg'_{Al} : Al^{\cdot}_{Mg}\}$, two pairs of defects and lastly three pairs of defects, that is, the same cluster configurations as invoked in section 3.2.1. These latter cluster cases include the effect of intra cluster defect-defect interactions but do not include longer range inter cluster interactions, as the defects are no longer repeated via periodic conditions.

3.2.3 Combined Energy Minimisation - Monte Carlo (CEMMC)

A comprehensive study of cation disorder in spinel is problematic; even within a single unit cell, when neglecting symmetry, there are 735471 possible configurations for disorder on the cation sub-lattice. Identifying and calculating the energies of each configuration would be a mammoth task. The CEMMC technique allows us to intelligently sample the possible degrees of disorder and through configurational averaging make predictions of macroscopic properties dependent upon these configurations. It has been demonstrated previously that the technique can simulate Al-Fe disorder involving uncharged defects in a study of $Ca_2Fe_xAl_{2-x}O_5$ brownmillerite over the whole compositional range $0 \leq x \leq 2.0$ [12, 69]. As is shown in the present study, the method is also successful in simulating systems containing charged defects. An overview of the Monte Carlo principle is provided in section 2.8, what follows is details as they apply to the specific problem under consideration.

Energy minimisation is used to obtain the energy and lattice properties for multiple arrangements for Mg and Al within a periodically repeated supercell (i.e. not just the four arrangements in section 3.2.1) constructed from either $1 \times 1 \times 1$ or $2 \times 1 \times 1$ unit cells of stoichiometric $MgAl_2O_4$ (which contain 56 and 112 ions respectively). The arrangements are generated using the Metropolis statistical sampling Monte Carlo technique [69] as follows. At a given iteration the system has the cation configuration μ of energy E_μ. Two randomly chosen cations are then exchanged forming a new configuration ν. The lattice is minimised and the new energy, E_ν, is calculated and the new configuration is adopted in place of the old with probability W:

$$\begin{aligned} W_{\mu\to\nu} &= \exp(-\tfrac{\Delta E}{kT}), \quad \Delta E > 0 \\ &= 1, \quad \Delta E < 0 \end{aligned} \tag{3.6}$$

where T is the simulation's target temperature, k is Boltzmann's constant and $\Delta E = E_\nu - E_\mu$.

Within this scheme the expectation value of the quantity Q is given by

$$\langle Q \rangle = \frac{\sum_\mu Q_\mu N_\mu}{\sum_\mu N_\mu}, \tag{3.7}$$

where Q takes the value Q_μ for configuration μ. The value N_μ is the number of times configuration μ was chosen, either because it had been swapped into from another configuration or because it was the incumbent configuration during a failed swap attempt [12, 69].

In order to generate different overall degrees of disorder different target tem-

peratures were employed (clearly a higher temperature gives rise to a greater overall degree of disorder). For each target temperature the system was first equilibrated for 1000 swap attempts then 6000 further attempts (as opposed to successful swaps) are made. Figure 3.2 shows the mean lattice energy of a single unit cell of spinel, averaged over 6000 swap attempts, after the indicated number of equilibration steps.

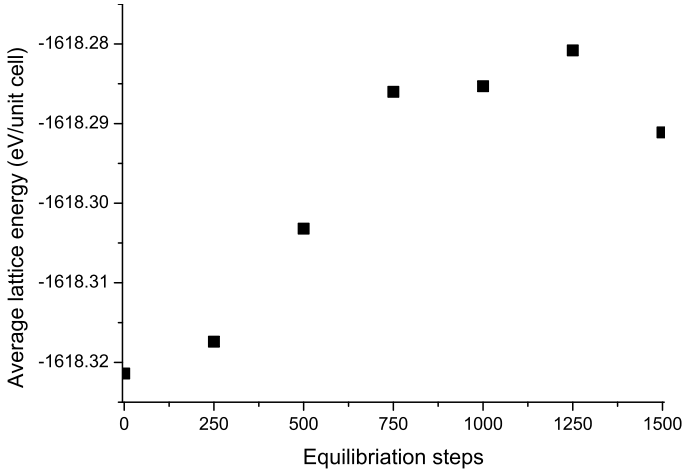

Figure 3.2: Mean lattice energy (eV) of a single unit cell of spinel over 6000 CEMMC swap attempts following the shown number of equilibration steps (at a target temperature of 2000K).

It is stressed that contributions to the free energy of the system by lattice vibrations are included only through the quasi-harmonic approximation, for the temperature at which potential parameters were fitted, that is room temperature. Therefore the simulation temperatures served only to generate different degrees of average disorder and correlate to the materials properties at room temperature, not at the simulation temperature. This implies that comparison should be made with experimental data derived from samples

which have been quenched rapidly thereby "freezing-in" disorder such as data from reference [117] (as opposed to *in situ* data which would require a molecular dynamics approach such as that used recently by Lavrentiev *et al.* [127]).

3.2.4 Mean Field Approximation

The mean field theory attempts to approximate the effect of all possible disorder by applying, between each pair of sites, a potential that is the mean of the potentials arising from all possible configurations. That is, the mean field approximation averages the potential at each lattice site with respect to the degree of disorder. While the computational ease of this method makes it desirable, it is flawed in two respects. First, it assumes all configurations are equally likely. Second, it assumes an averaged ion charge per site commensurate with the degree of disorder. The mean field analysis was conducted using the GULP code [128].

3.2.5 Periodic Boundary Density Functional Calculations

In addition to pair potential simulations density functional calculations (DFT) (see section 2.9) were undertaken using the plane wave code CASTEP [129]. Due to computational restrictions calculations could only be carried out on the four configurations described in section 3.2.1, in a single unit cell. The

system was modelled using the GGA employing the PBE functional [93] and also assuming the LDA using the CA-PZ functional [131,132]. In both cases ultrasoft pseudopotentials were employed with a 380 eV plane wave cut-off. The Brillouin zone was sampled on a 4x4x4 Monkhorst-Pack grid [96].

The aim of carrying out these quantum mechanical simulations is to provide a direct comparison to pair potential simulation (specifically those of section 3.2.1) and as such act as a further test of the potentials.

3.3 Lattice Parameter Variation with Disorder

3.3.1 Periodic Boundary Condition Simulations Using DFT and Pair Potentials

Figure 3.3 compares the predicted variation in lattice parameter with increasing antisite disorder found via density functional and pair potential calculation using identical unit cell repeat units (see section 3.2.5). The GGA and LDA DFT calculations (square symbols and triangle symbols) overestimate the perfect spinel cell volume by 0.85% and 0.20% respectively (as can be seen from the comparison with the experimental data; crosses and star). A comparison of the DFT and pair potential techniques is nevertheless useful; both predict that the lattice parameter decreases slowly as the numbers of antisite pairs is increased. The GGA calculation shows a no-

ticeably greater fall in lattice parameter between 0 and 1 antisite pair than between subsequent points, which is not reproduced either by the LDA or by the pair potentials. It is, however, important to note that for all cases the total change in lattice parameter over the range considered is less than 0.25%.

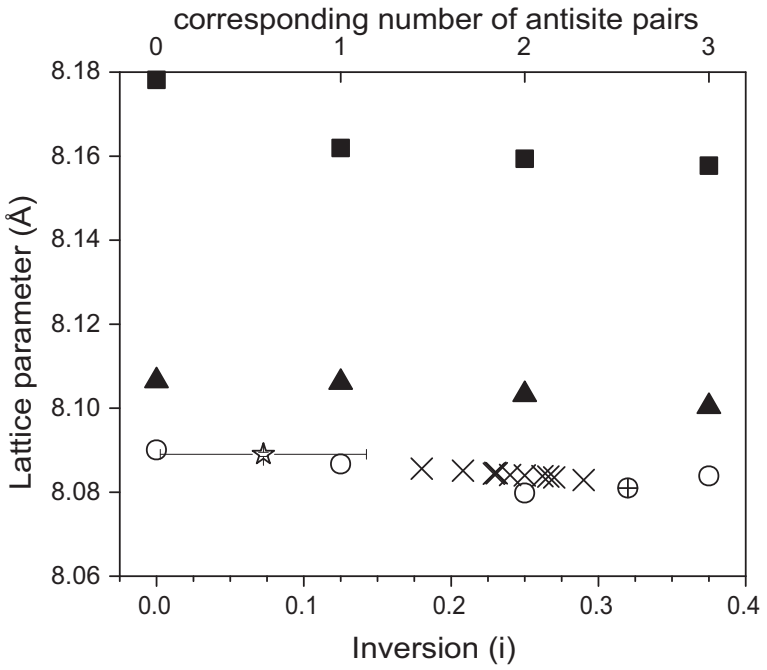

Figure 3.3: Variation in lattice parameter with inversion for specific defect cluster configurations containing, respectively, 0, 1, 2 and 3 antisite pairs. The solid square symbols correspond to GGA DFT calculations, the solid triangles to LDA DFT calculations, the open circles to pair potential calculations and the experimental data is represented as crosses [117], crossed circles [118] (synthetic samples) and by a star [28] (natural sample).

3.3.2 The Mean Field Approach

Results of the mean field analysis of the variation in lattice parameter are presented in figure 3.4. Although this technique correctly predicts a negative gradient in lattice parameter as a function of inversion, the magnitude of this gradient is many times greater than that of the experimental data. This discrepancy is the result of overestimating the Coulomb interactions as a function of increasing disorder, which leads to lattice contraction.

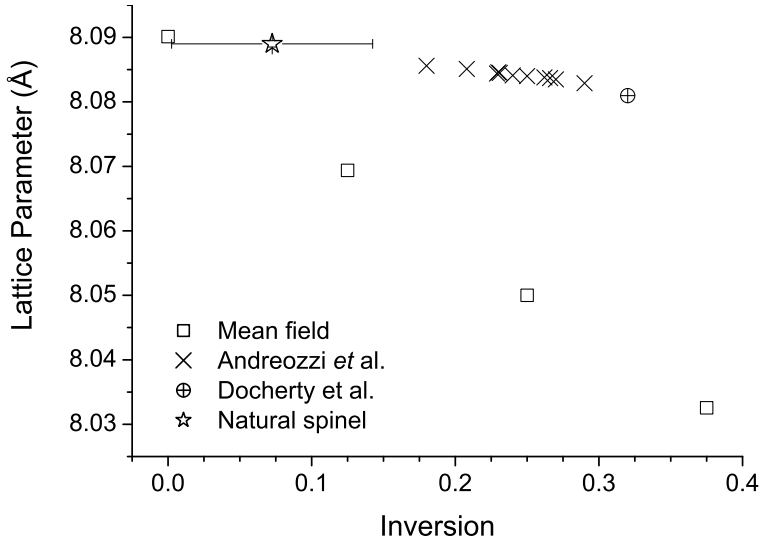

Figure 3.4: Variation in lattice parameter with inversion predicted using a mean field analysis. This shows significant deviation in slope from the experimental data [28, 117, 118].

3.3.3 Defect Volume Predictions

Figure 3.5 shows the results generated via the technique described in section 3.2.2. As it relies on multiplying the volume of a chosen defect configuration by the defect concentration, it implicitly contains an assumption as to what this defect should be. Here, results are shown assuming: an isolated pair of Mg'_{Al} and $Al^{\cdot}_{Mg}$ defects, then progressively larger clusters of 1, 2 and 3 nearest neighbour antisite pairs (as previously emphasised these configurations are the same as those used for the DFT and equivalent pair potential cluster calculations). The predicted volumes are reported in table 3.6.

Table 3.6: Defect volumes as predicted from equation 3.3.

Cluster	Volume (Å^3)
$Al^{\cdot}_{Mg}$	-0.683
Mg'_{Al}	0.606
$\{Al^{\cdot}_{Mg}{:}Mg'_{Al}\}$	-0.348
$2\{Al^{\cdot}_{Mg}{:}Mg'_{Al}\}$	-0.885
$3\{Al^{\cdot}_{Mg}{:}Mg'_{Al}\}$	-1.419

As with the other techniques this approach is also able to reproduce the small negative gradient of the experimental data. Within these defect volume predictions a trend can be seen, in that the results become progressively closer to the experimental data on synthetic materials as the size of the cluster increases (see figure 3.5). Beginning with isolated defects the volumes cancel out to a significant extent (see table 3.6) suggesting negligible change in the lattice parameter with increasing disorder. We would, however, only

expect the defects to be isolated for the very lowest values of inversion, i, when configurational entropies dominate. Conversely the experimental data for synthetic materials correspond to a defect regime where defect-defect interactions are inevitably significant. Indeed, even the data for the natural spinel compares best to the prediction assuming cluster formation.

These results suggest that a *modestly sized* cluster can represent the majority of the effect that defect-defect interactions have on lattice parameter change. Of course, it should be noted that in this system the change in lattice parameter is rather small, thus this cluster approximation does not have to account for a great change in lattice parameter.

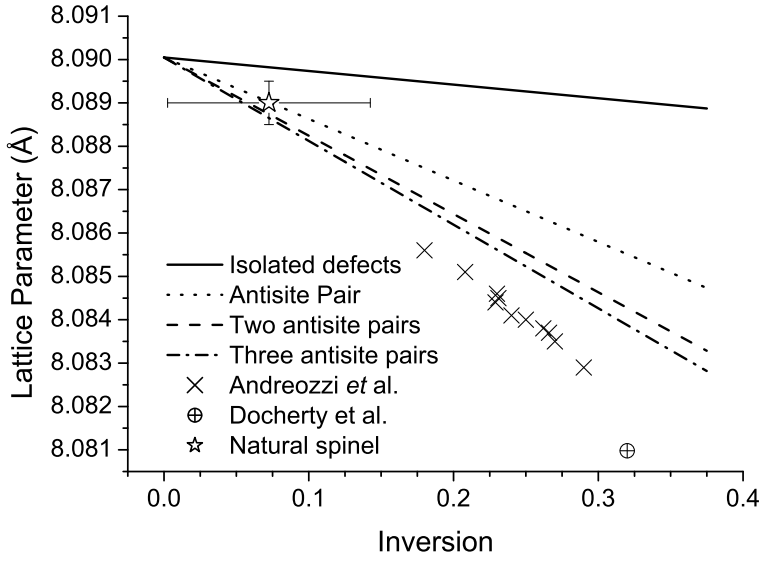

Figure 3.5: Variation in lattice parameter with inversion as predicted using defect volume analysis. The experimental data of Andreozzi *et al.* [117], Docherty *et al.* [118] and Hafner *et al.* [28] are included for comparison.

3.3.4 Combined Energy Minimisation - Monte Carlo (CEMMC) Predictions

In practice the lattice can be considered to contain many clusters of varying sizes in differing proportions, all of which interact. The aim of the CEMMC technique is to sample a representative distribution of defect configurations that can reproduce the effect of such a complex system. It was found (see figure 3.6) that the method was able to reproduce the experimental data better than the other methods. Interestingly the gradient of the results reproduced using the smaller supercell ($1 \times 1 \times 1$) is slightly greater than that of the experimental data for synthetic materials. Results derived using the $2 \times 1 \times 1$ supercell lie very close to these experimental results. Considering the analysis of the defect volume method, this suggests that defect-defect interactions are exaggerated by the confined $1 \times 1 \times 1$ supercell. Extension to a larger system size, such as a $2 \times 2 \times 1$ supercell, though desirable, is prohibited by the computational cost.

The CEMMC method allows us to predict the variation in lattice parameter over a wider range of inversion parameter than studied in [117, 118]. Furthermore, whereas the mean field and defect volume analysis necessarily produce linear relationships for lattice parameter as a function of inversion, the CEMMC method is capable of predicting a nonlinear variation. Nonlinearity is indeed observed (figure 3.6), though its extent is modest. The shape of the curve predicted from the CEMMC data can be rationalised in terms of the defect volume results. At low degrees of disorder the constituent

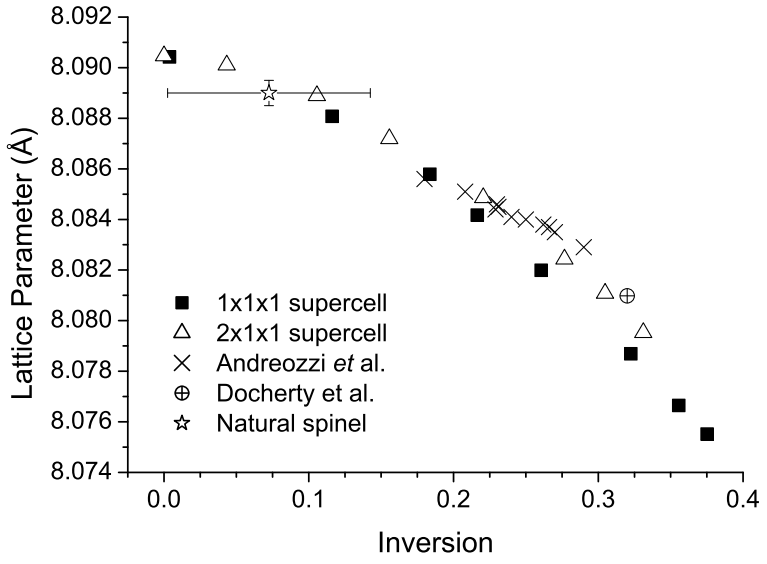

Figure 3.6: Variation in lattice parameter with inversion as predicted using CEMMC analysis. The experimental data of Andreozzi *et al.* [117], Docherty *et al.* [118] and Hafner *et al.* [28] are included for comparison.

defects are likely to be in pairs (or even isolated) for entropic reasons. The variation of lattice parameter with inversion will therefore tend to follow the second line in figure 3.5. As defect concentrations increase, the variation will tend towards the lower two lines in figure 3.5. The result is a downwards curvature as observed in figure 3.6.

3.4 Oxygen Positional Parameter Variation with Disorder

Oxygen positions in $MgAl_2O_4$ are listed in table 3.1 the positional (u) parameter is a shift from idealised positions away from the neighbouring Mg^{2+} ion and toward the three neighbouring Al^{3+} ions. Within the simulations discussed in this chapter oxygen is described via the incorporation of a shell model (see section 2.5). The simulation returns positions of both the core and shell. These positions can be compared with the x-ray diffraction obtained data of Andreozzi *et al.* [117]. It might be expected that the core positions should better fit the x-ray diffraction data because within the model the shell represents only the outermost valence electrons whereas the core includes not only the nucleus but also the majority of the electron density and should thus have a larger cross section for x-ray adsorption than the shell. Nevertheless both the core and shell positions are shown in figures 3.7-3.9, and in addition a weighted average of the core and shell positions taking into account the relative share of the electrons of the O^{2-} ion assigned to the cores and shells.

This average takes the form of equation 3.8:

$$\langle u \rangle = \frac{7.2u_{core} + 2.8u_{shell}}{10} \tag{3.8}$$

3.4.1 The Mean Field Approach

Figure 3.7 shows the results obtained for the u parameter via mean field calculations. The mean field is able to reproduce correctly the trend in the experimental data. As expected the core positions are closer to the experimental data than the shell positions with the weighted average coinciding closely with the numbers of Andreozzi *et al.* [117].

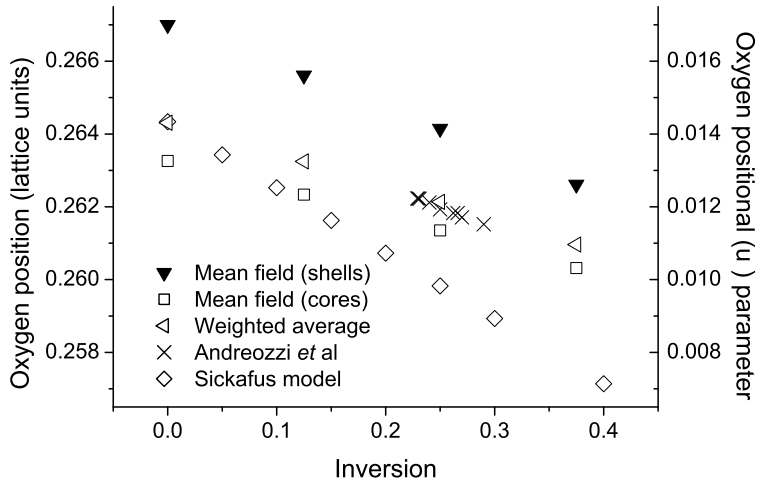

Figure 3.7: Variation in oxygen positional (u) parameter with inversion predicted using a mean field analysis. Results are compared with experimental data [117] and the model of Sickafus *et al.* [38].

3.4.2 Combined Energy Minimisation - Monte Carlo (CEMMC) Predictions

In contrast with the results for the lattice parameter the CEMMC does not improve upon the mean field approximation in its prediction of the u parameter. It should be noted that the overall change in u parameter over the data is small, the change across the experimental data of Andreozzi *et al.* amounts to a shift in atomic position of just 0.006 Å however this is larger than the corresponding shift in lattice parameter (0.003 Å). Results have been divided according to supercell size with results for the 1x1x1 supercell in figure 3.8 and those for the 2x1x1 supercell in figure 3.9. Similarly to section 3.3.4, the results of the 1x1x1 and 2x1x1 supercell differ only by a small fraction. Again, the core positions more closely reflect the experimental data than the shells. Though the total change in u parameter is small in the range being considered it is clear that this change is being underestimated by the CEMMC technique. In contrast the Sickafus model, which considers only averages rather than specific configurations, is able to reproduce the gradient closely.

As well as depending on the balance of the sizes of the ions occupying the tetrahedral and octahedral sites (or in terms of the simulations the shape of the Al^{3+}-O^{2-} and Mg^{2+}-O^{2-} potentials) the u parameter was found to be sensitive to the shell model parameters.

Figure 3.10 illustrates results obtained via CEMMC and mean field analysis

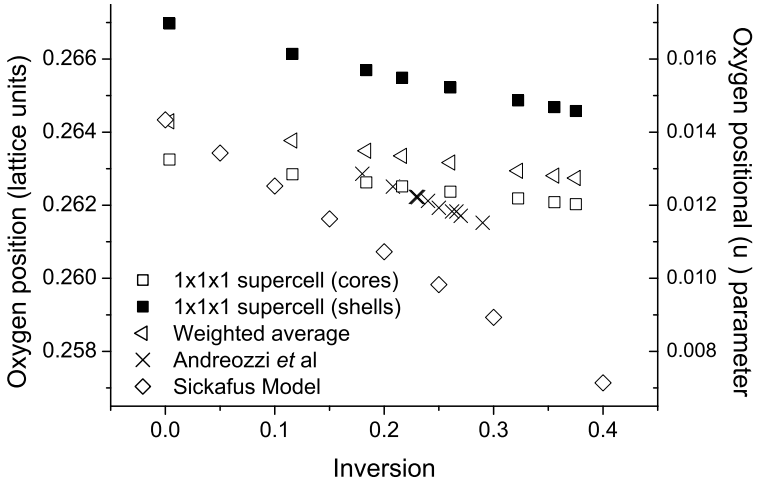

Figure 3.8: Variation in oxygen positional (u) parameter with inversion predicted using a the CEMMC methodology with a 1x1x1 supercell. Results are compared with experimental data [117] and the model of Sickafus *et al.* [38].

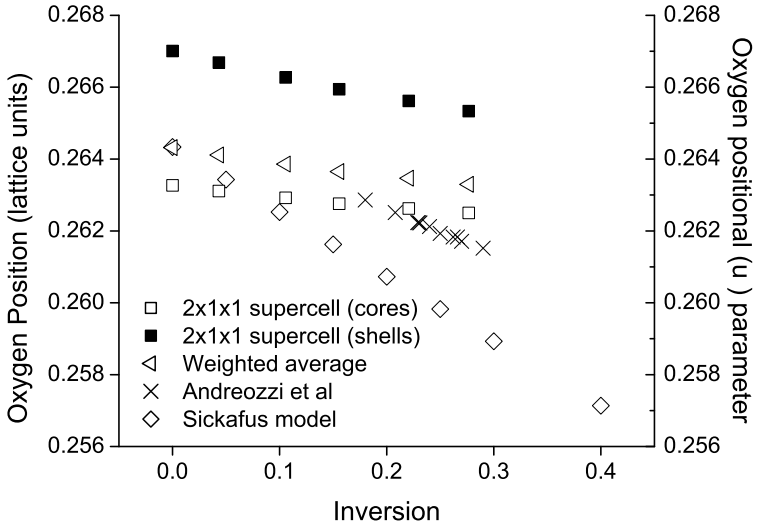

Figure 3.9: Variation in oxygen positional (u) parameter with inversion predicted using a the CEMMC methodology with a 2x1x1 supercell. Results are compared with experimental data [117] and the model of Sickafus *et al.* [38].

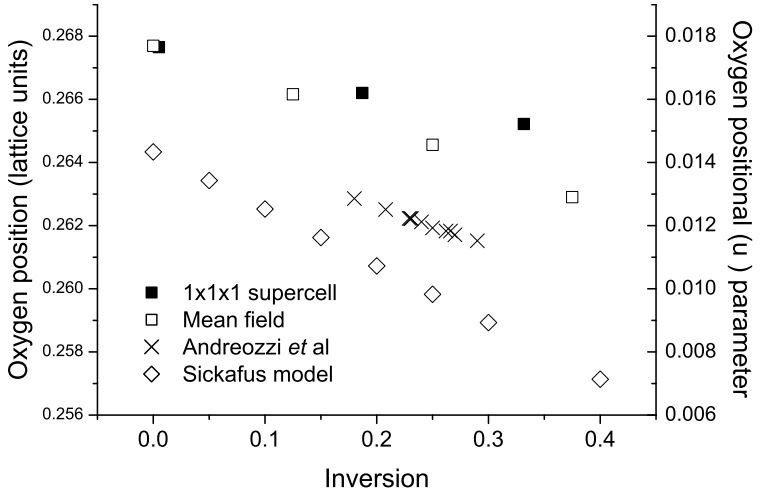

Figure 3.10: Variation in oxygen positional (u) parameter with inversion predicted using a the CEMMC and mean field methodologies. Oxygen ions are modeled without a shell. Results are compared with experimental data [117] and the model of Sickafus *et al.* [38].

of u parameter when the oxygen ions are treated without a shell. As might be expected the displacement of the oxygen ions from ideal positions is greater in this case than in figures 3.7-3.9, however the gradient of the trend lines closely mirror the experimental data. It is possible that a more complicated shell model, such as the breathing shell [81] would better model the balance between the changing position and size of the oxygen site.

3.5 Summary

$MgAl_2O_4$ is usually described as having a normal spinel structure, in which case, all the Mg^{2+} ions should occupy all of the tetrahedral sites and the Al^{3+} ions should occupy all of the octahedral sites. In reality there is a significant and variable degree of mixing [34] between these cations. This is known as antisite disorder and for $MgAl_2O_4$ results in a modest reduction of both the lattice parameter and u parameter. The degree of mixing (inversion) depends on the thermal history of the material.

Here we have described four approaches to modelling the effect of antisite disorder on the lattice parameter. These increase in statistical and/or computational complexity from: a simple mean field method, a restricted configurational supercell approach, a calculation of defect volume applied to a consideration of defect concentration and finally configurational averaging via a Monte Carlo simulation. Both the CEMMC and mean field methods were also used to model u parameter variation with inversion. In each case

forces between ions were described by pair potentials although the supercell calculations were repeated using GGA and LDA DFT methods.

In terms of the lattice parameter, the CEMMC method, which uses a Monte Carlo approach to generate defect configurations and statistically average, best reproduced the experimental data. These results suggest a slight non-linear variation in lattice parameter as a function of inversion which can also be seen in recent calculations by Seko *et al.* [113]. Such behavior can be anticipated from the defect volume calculations that suggest greater variation in lattice parameter with increasing cluster formation (as would inevitably occur with greater degrees of inversion). The mean field approach that assumes an average distribution of Al^{3+} and Mg^{2+} ions commensurate with a given inversion is shown to yield much less satisfactory results.

The CEMMC and mean field descriptions closely reproduce the experimental values for the u parameter. In contrast with the variation in lattice parameter calculations, however, the CEMMC method fails to improve upon the less computationally demanding approach. It is worth noting that the value of the mean field results are somewhat dubious as the technique is incorrectly modelling the change in lattice parameter (see figure 3.4), thus the u parameters are those of the oxygen ions in an under sized unit cell. The results obtained using equation 3.2 seem to confirm the hypothesis that the ratio of the cation radii is the most significant factor behind the change in u parameter with inversion.

In conclusion, the results demonstrate that a statistically derived distribution

of charged antisite defects can reproduce the experimentally observed variation in lattice parameter. A method based on pair potentials is thus able to model certain residual defects in $MgAl_2O_4$ that are formed as a consequence of radiation damage. It does not, of course, establish that the methodology is able to model the dynamical processes whereby the defects are formed. As a step towards this we will, in subsequent chapters, model ion migration in this system.